Molecular Insights on Kinetic Stabilization of Amorphous Solid Dispersion of Pharmaceuticals

Supplementary Information

Vladislav Aulich[a], *Jan Ludík*,[a] *Michal Fulem*,[a] *Ctirad Červinka*[a,*]

[a] Department of Physical Chemistry, University of Chemistry and Technology Prague, Technická 5, CZ-166 28 Prague 6, Czech Republic

*Corresponding author: cervinkc@vscht.cz

S1. Excess properties

This section contains additional simulation results on excess molar volumes and excess enthalpies of bulk mixtures of target API and polymers. Numerical values of calculated excess properties and a benchmark plot of those are listed below.

Table S1. Excess molar volumes V^E (in $cm^3\ mol^{-1}$) and excess molar enthalpies H^E (kJ mol^{-1}) of simulated mixtures of target API and polymers at various compositions and temperatures.

		PLA			
		300 K		500 K	
API	x_{API}	V^E	H^E	V^E	H^E
CBZ	0.85	−5.5±0.3	0.6 ± 0.3	0.9±0.5	4.7 ± 0.5
	0.92	−3.5±0.2	0.5 ± 0.2	0.6±0.3	3.2 ± 0.3
	0.95	−2.3±0.2	−0.1 ± 0.2	0.2±0.2	2.7 ± 0.2
IBU	0.85	−9.6±0.4	−1.3 ± 0.4	0.3±0.5	3.3 ± 0.5
	0.92	−6.5±0.3	−0.3 ± 0.2	0.1±0.3	2.6 ± 0.3
	0.95	−5.3±0.2	0.2 ± 0.2	−0.1±0.2	2.1 ± 0.2
IND	0.85	−7.3±0.3	5.2 ± 0.3	−1.2±0.6	8.6 ± 0.7
	0.92	−3.9±0.2	4.7 ± 0.2	−1.7±0.3	6.4 ± 0.3
	0.95	−3.0±0.2	2.0 ± 0.2	−2.0±0.3	3.5 ± 0.4
NAP	0.85	−5.0±0.3	4.4 ± 0.3	3.3±0.5	7.5 ± 0.5
	0.92	−2.2±0.2	3.9 ± 0.3	2.6±0.3	6.3 ± 0.3
	0.95	−1.8±0.1	3.4 ± 0.1	1.5±0.2	4.7 ± 0.2

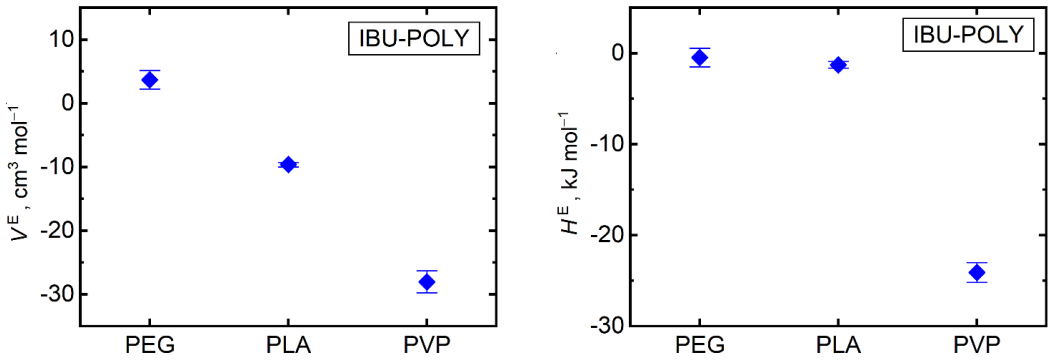

Figure S1. Excess molar volumes (V^E) and enthalpies H^E (in kJ mol^{-1}) of simulated mixtures of IBU and target API at equimolar composition and temperature 300 K.

S2. Structural aspects

This section contains additional simulation results on structural characterization of bulk mixtures of target API and polymers. Plots of small-angle neutron scattering profiles, radial distribution functions, spatial coordination functions and a comparison of coordination numbers are given below.

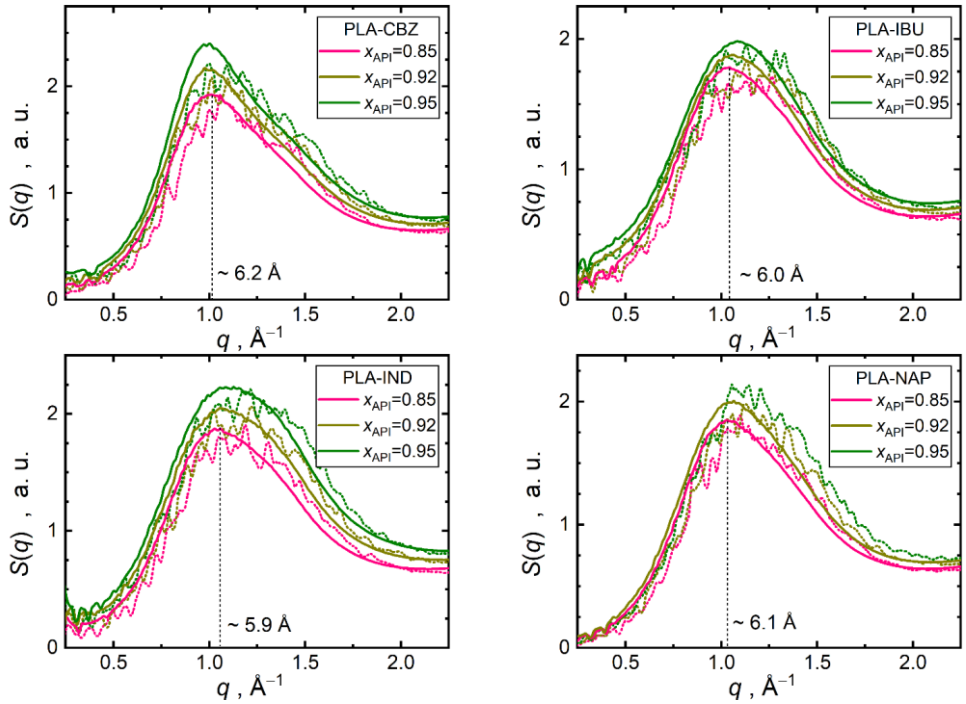

Figure S2. Static structure factors $S(q)$ simulating the small-angle neutron diffraction for individual considered dispersions of API and polymers, data for 500 K and 300 K are given with solid and dashed lines, respectively.

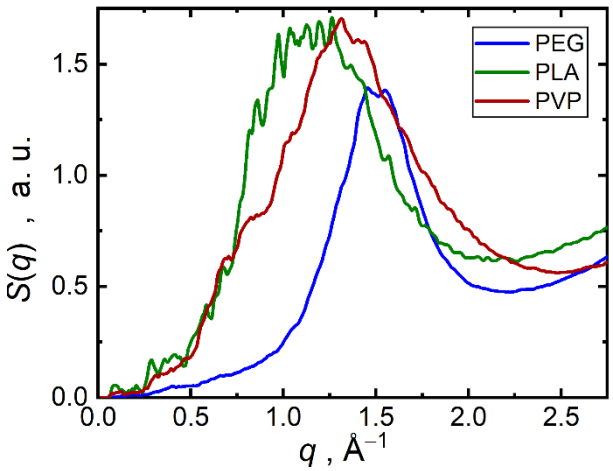

Figure S3. Static structure factors $S(q)$ simulating the small-angle neutron diffraction for dispersions of IBU (x_{IBU}=0.85) with individual polymers at 300 K.

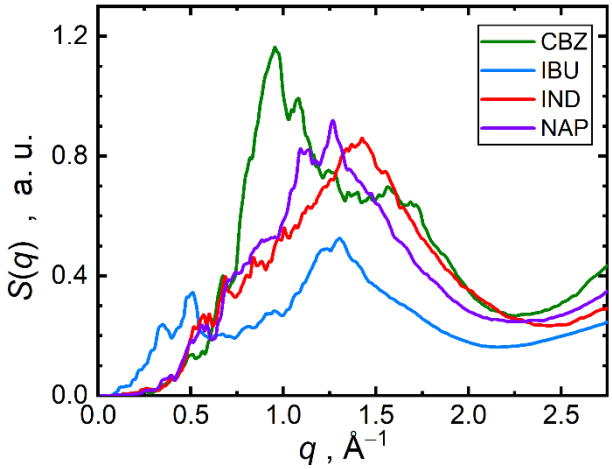

Figure S4. Static structure factors $S(q)$ simulating the small-angle neutron diffraction for individual considered pure amorphous API at 300 K.

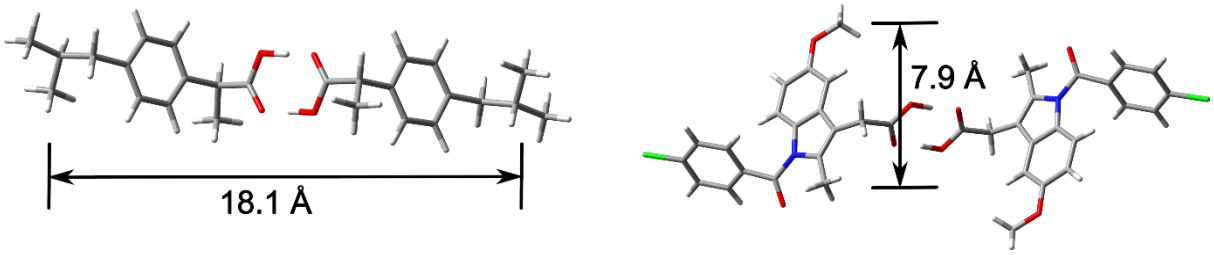

Figure S5. Characteristic dimensions of optimized geometries of the closest carboxyl-dimers of ibuprofen and indomethacin molecules.

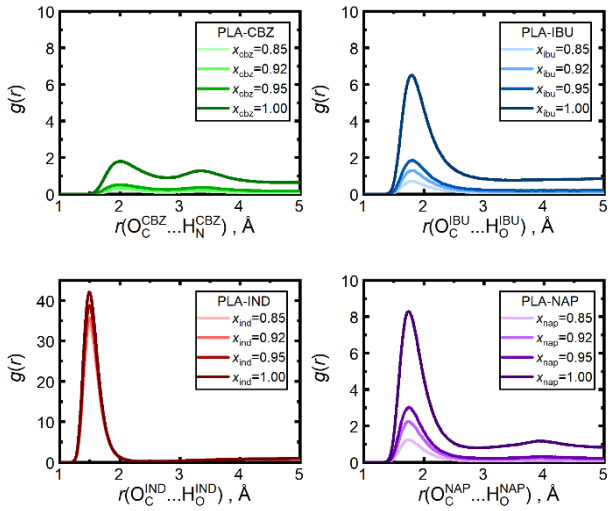

Figure S6. Radial distribution functions $g(r)$ for intermolecular contacts of the API carboxyl/amide hydrogen atom (H_O/H_N) with the API carbonyl oxygen atom (O_C) in pure amorphous API and API-PLA mixtures simulated at 500 K. Signals from the mixtures are renormalized so that the unity value always corresponds to the average contact counts in neat bulk API.

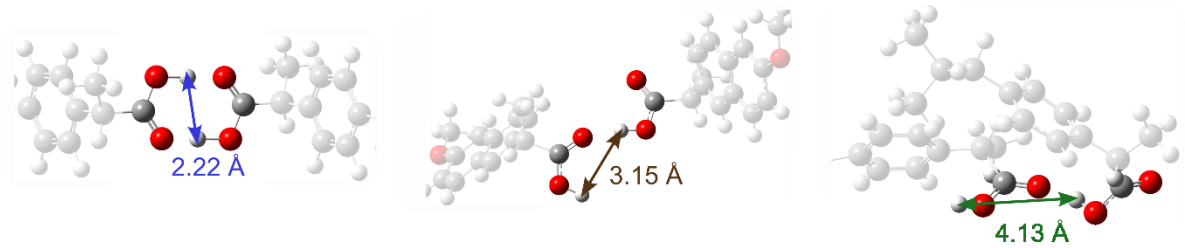

Figure S7. Illustration of the closest carboxyl dimers and carboxyl chain units representing important packing motifs of bulk API systems with the $H_O \cdots H_O$ contact distances taken from experimental crystal structures (first two configurations) and simulated bulk liquid phase (last configuration).

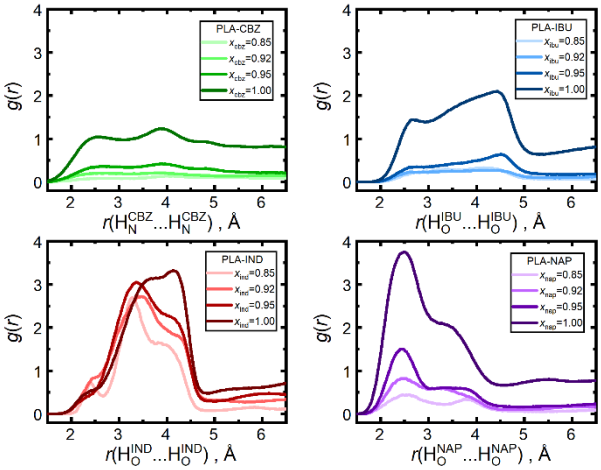

Figure S8. Radial distribution functions for contacts of the API carboxyl/amide hydrogen atoms (H_O/H_N) in API-PLA mixtures and pure amorphous API simulated at 300 K.

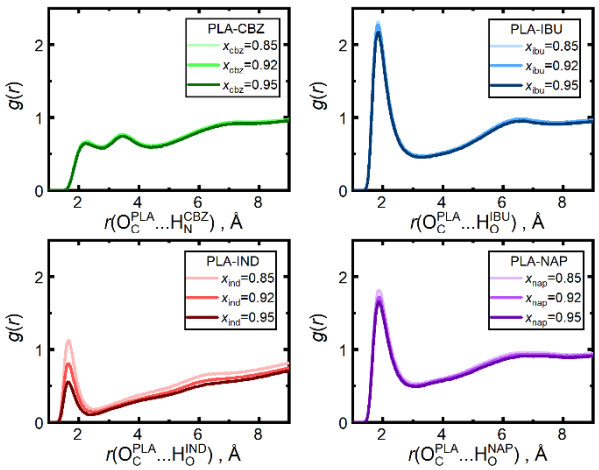

Figure S9. Radial distribution functions for contacts of the API carboxyl/amide hydrogen atom (H_O/H_N) with the PLA carbonyl oxygen atom (O_C) in API-PLA mixtures simulated at 500 K.

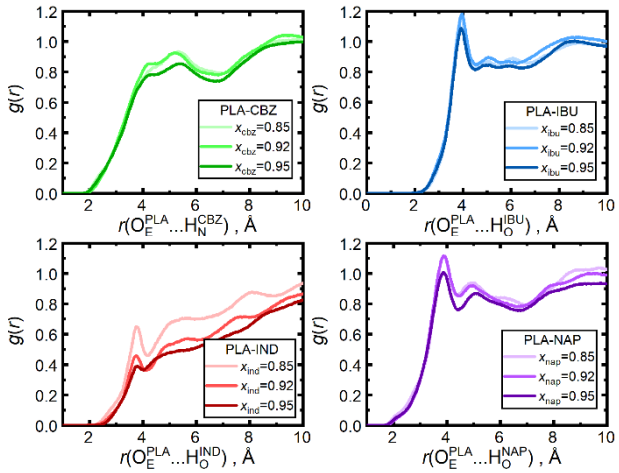

Figure S10. Radial distribution functions for contacts of the API carboxyl/amide hydrogen atom (H_O/H_N) with the PLA ester oxygen atom (O_E) in API-PLA mixtures simulated at 300 K.

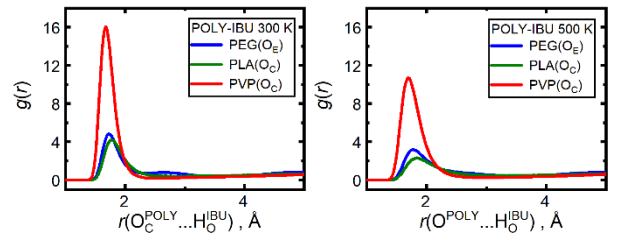

Figure S11. Radial distribution functions for contacts of the IBU carboxyl hydrogen atom (H_O) with an oxygen atom being the most active acceptor of the hydrogen bond in the polymer chains in IBU-POLY mixtures simulated at 300 K and at 500 K.

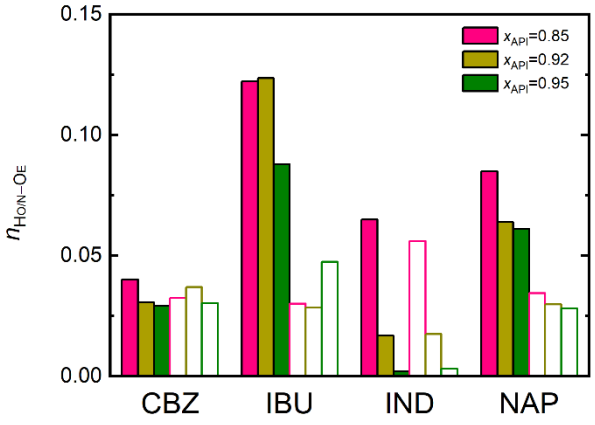

Figure S12. Coordination numbers for intermolecular contacts of the API carboxyl/amide hydrogen atom (H_O/H_N) with the PLA ester oxygen atom (O_E) in API-PLA mixtures simulated at 300 K (full columns) and 500 K (empty columns). Values correspond to the radius of the first coordination shell of the H_O/H_N-O_C contacts as the radius for these H_O/H_N-O_E contacts is excessively large.

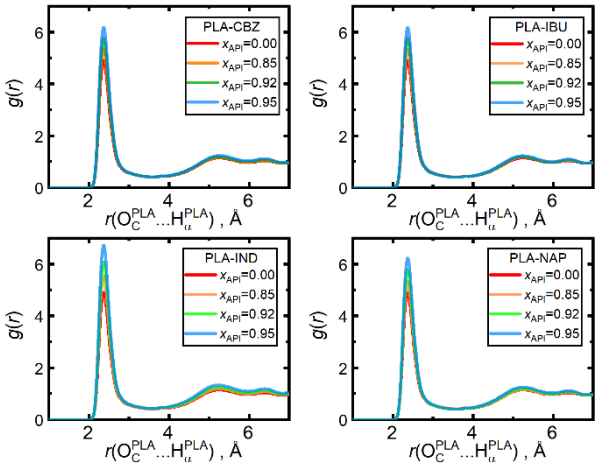

Figure S13. Radial distribution functions for intermolecular contacts of PLA fragments – between the carbonyl (O_C) atom and the hydrogen atom bound to the α-carbon being next to the carboxyl group (H_α) in the polymer chains in API-PLA mixtures and pure PLA simulated at 300 K.

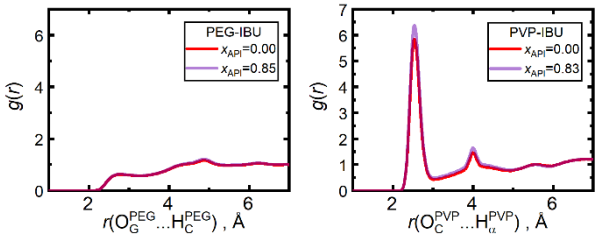

Figure S14. Radial distribution functions for intermolecular contacts of polymer fragments – between the ether (O_G) atom and an adjacent hydrogen (H_C) atom in PEG or the carbonyl oxygen (O_C) atom and the hydrogen atom bound to the α-carbon being next to the carboxyl group (H_α) in PVP in IBU-POLY mixtures and pure polymers simulated at 300 K.

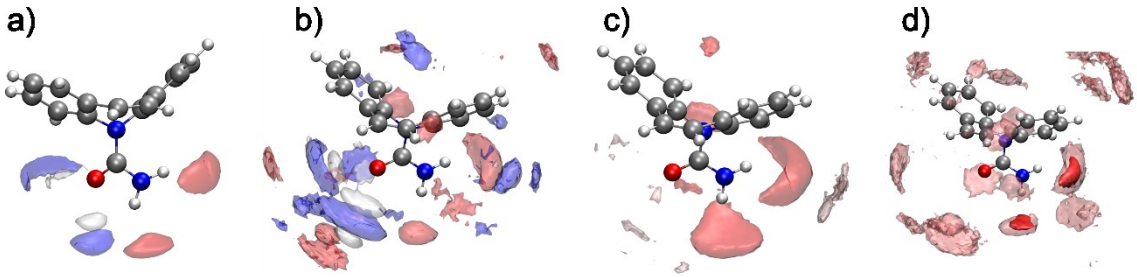

Figure S15. Spatial distribution functions around a fixed amide frame of CBZ molecules simulated at 300 K. Image legend: a) pure amorphous CBZ – red, blue, and white surfaces depict distribution of O_C, N_H, and H_N atoms from neighboring CBZ molecules, respectively, all isovalues equal to 13; b) CBZ-PLA mixture with x_{API}=0.85 – same coloring and atom types as in a); c) the same CBZ-PLA mixture – dark red and light red surfaces depict distribution of O_C and O_E atoms from neighboring PLA molecules, respectively, all isovalues equal to 3; d) the same CBZ-PLA mixture – dark red and light red surfaces depict distribution of O_C atoms from neighboring PLA and CBZ molecules, respectively, all isovalues equal to 8.

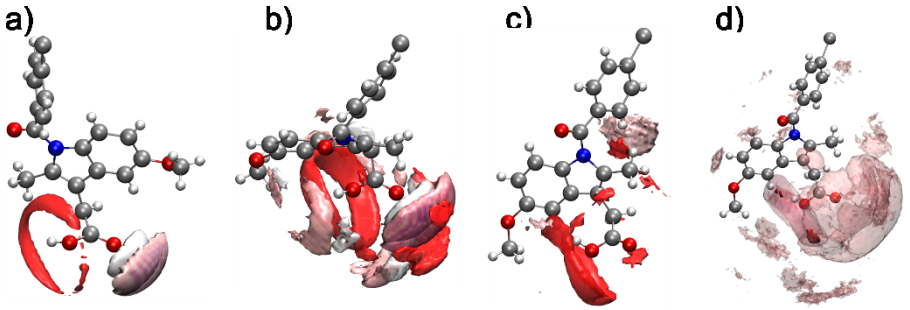

Figure S16. Spatial distribution functions around a fixed carboxyl frame of IND molecules simulated at 300 K. Image legend: a) pure amorphous IND – dark red, light red, and white surfaces depict distribution of O_C, O_H, and H_O atoms from neighboring IND molecules, respectively, all isovalues equal to 40; b) IND-PLA mixture with x_{API}=0.85 – same coloring and atom types as in a); c) the same IND-PLA mixture – dark red and light red surfaces depict distribution of O_C and O_E atoms from neighboring PLA molecules, respectively, all isovalues equal to 2.3; d) the same IND-PLA mixture – dark red and light red surfaces depict distribution of O_C atoms from neighboring PLA and IND molecules, respectively, all isovalues equal to 25.

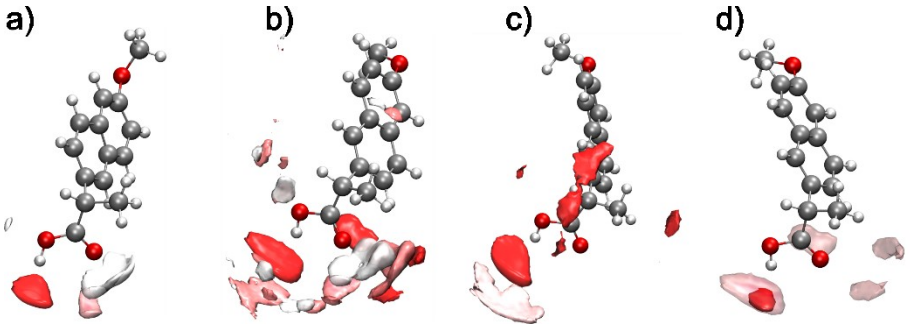

Figure S17. Spatial distribution functions around a fixed carboxyl frame of NAP molecules simulated at 300 K. Image legend: a) pure amorphous NAP – dark red, light red, and white surfaces depict distribution of O_C, O_H, and H_O atoms from neighboring NAP molecules, respectively, all isovalues equal to 20; b) NAP-PLA mixture with x_{API}=0.85 – same coloring and atom types as in a); c) the same NAP-PLA mixture – dark red and light red surfaces depict distribution of O_C and O_E atoms from neighboring PLA molecules, respectively, all isovalues equal to 4; d) the same NAP-PLA mixture – dark red and light red surfaces depict distribution of O_C atoms from neighboring PLA and NAP molecules, respectively, all isovalues equal to 28.

S3. Non-covalent interaction analysis

This section contains results of the quantum-chemical NCI analysis and related reduced-density gradient plots with a graphical legend focusing on the center of the most intensive interactions.

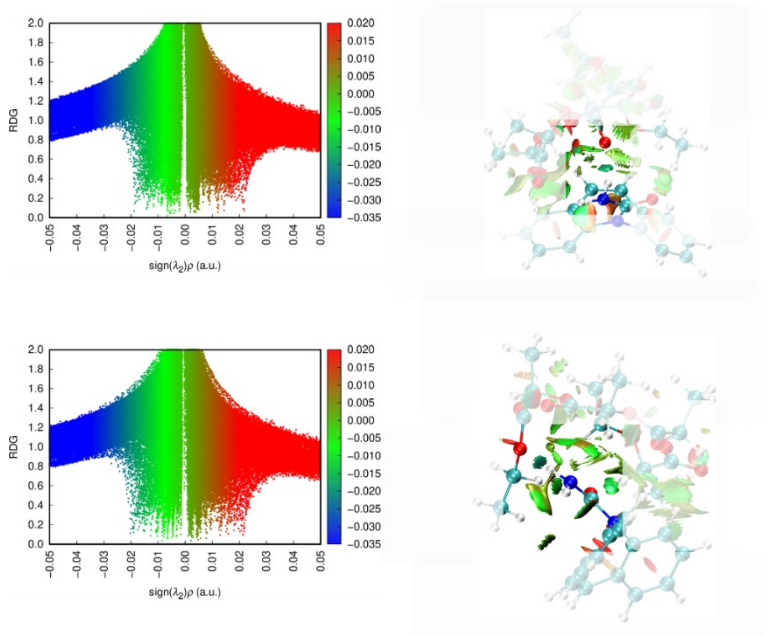

Figure S18. Analysis of non-covalent interactions of a PLA oligomer surrounding the amide moiety of CBZ in terms of critical points of the reduced density gradient plot and the signed electron density. Top row – conformation with a strong $H_N^{CBZ}…O_C^{PLA}$ hydrogen bond (dark blue RDG isosurface); Bottom row – conformation with a weak $H_N^{CBZ}…O_E^{PLA}$ hydrogen bond (light blue RDG isosurface). Attractive dispersion interactions depicted with green isosurfaces, repulsive interactions depicted with yellow to red shades.

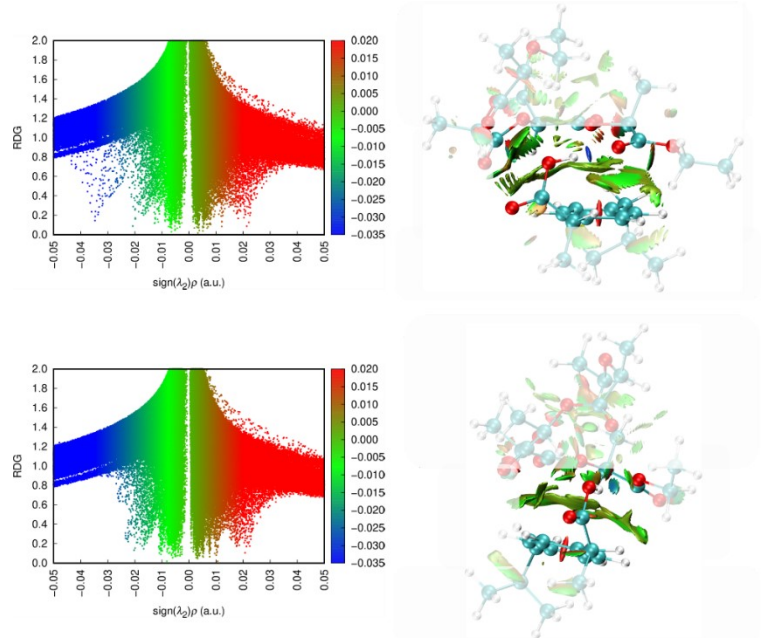

Figure S19. Analysis of non-covalent interactions of a PLA oligomer surrounding the carboxyl moiety of IBU in terms of critical points of the reduced density gradient plot and the signed electron density. Top row – conformation with a strong $H_O^{IBU}…O_C^{PLA}$ hydrogen bond (dark blue RDG isosurface); Bottom row – conformation with a weak $H_O^{IBU}…O_E^{PLA}$ hydrogen bond (light blue RDG isosurface). Attractive dispersion interactions depicted with green isosurfaces, repulsive interactions depicted with yellow to red shades.

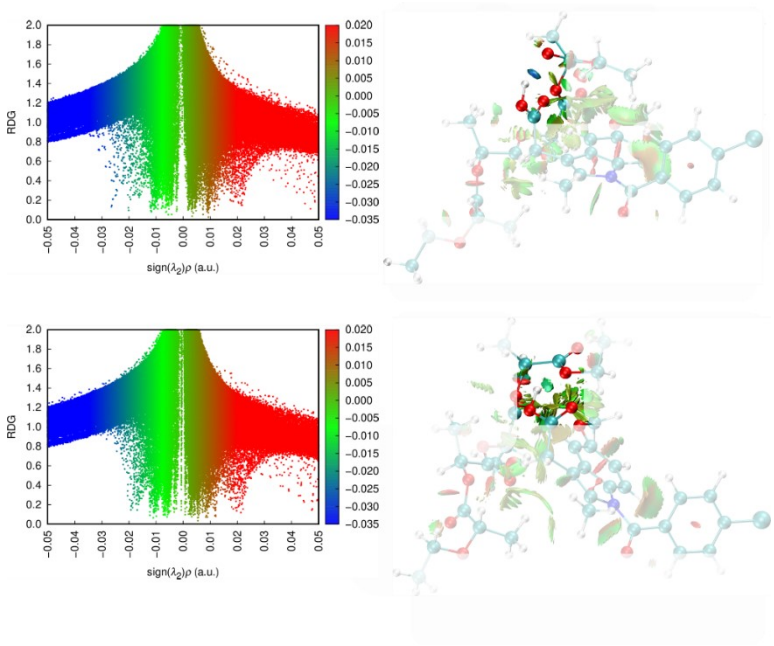

Figure S20. Analysis of non-covalent interactions of a PLA oligomer surrounding the carboxyl moiety of IND in terms of critical points of the reduced density gradient plot and the signed electron density. Top row – conformation with a strong $H_O^{IND}…O_C^{PLA}$ hydrogen bond (dark blue RDG isosurface); Bottom row – conformation with a weak $H_O^{IND}…O_E^{PLA}$ hydrogen bond (light blue RDG isosurface). Attractive dispersion interactions depicted with green isosurfaces, repulsive interactions depicted with yellow to red shades.

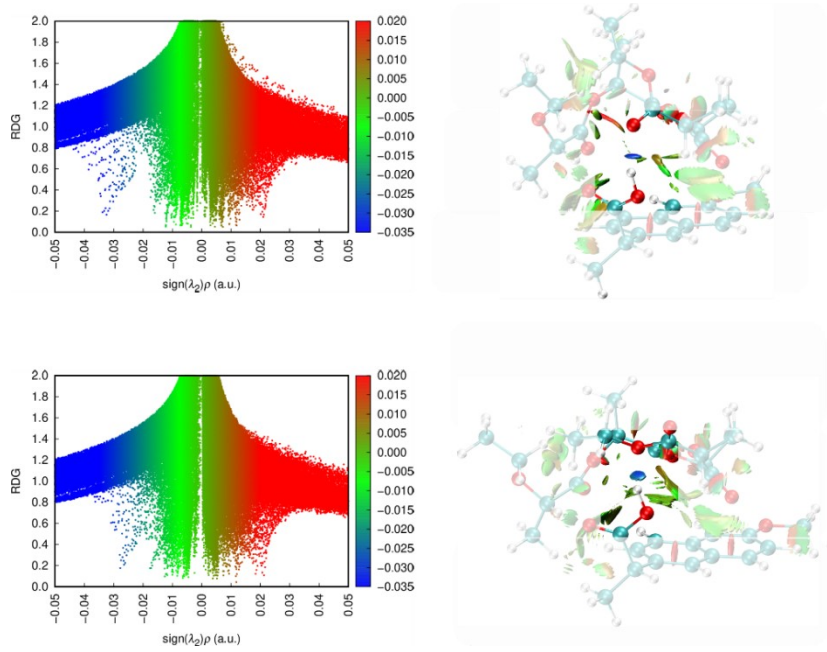

Figure S21. Analysis of non-covalent interactions of a PLA oligomer surrounding the carboxyl moiety of NAP in terms of critical points of the reduced density gradient plot and the signed electron density. Top row – conformation with a strong $H_O^{NAP}…O_C^{PLA}$ hydrogen bond (dark blue RDG isosurface); Bottom row – conformation with a weak $H_O^{NAP}…O_E^{PLA}$ hydrogen bond (light blue RDG isosurface). Attractive dispersion interactions depicted with green isosurfaces, repulsive interactions depicted with yellow to red shades.

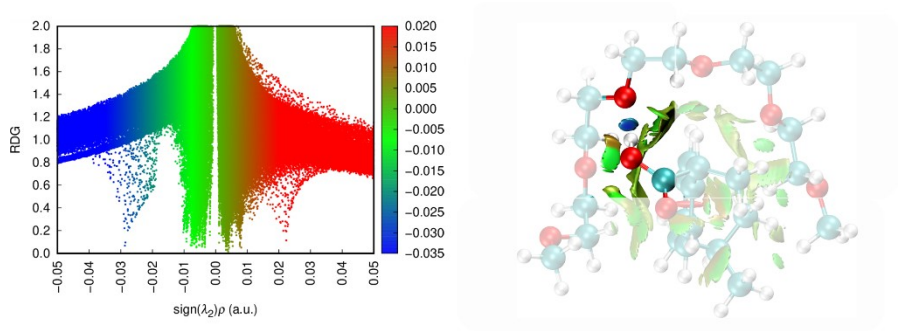

Figure S22. Analysis of non-covalent interactions of a PEG oligomer surrounding the carboxyl moiety of IBU in terms of critical points of the reduced density gradient plot and the signed electron density. Conformation with a $H_O^{IBU}…O_E^{PEG}$ hydrogen bond (blue RDG isosurface). Attractive dispersion interactions depicted with green isosurfaces, repulsive interactions depicted with yellow to red shades.

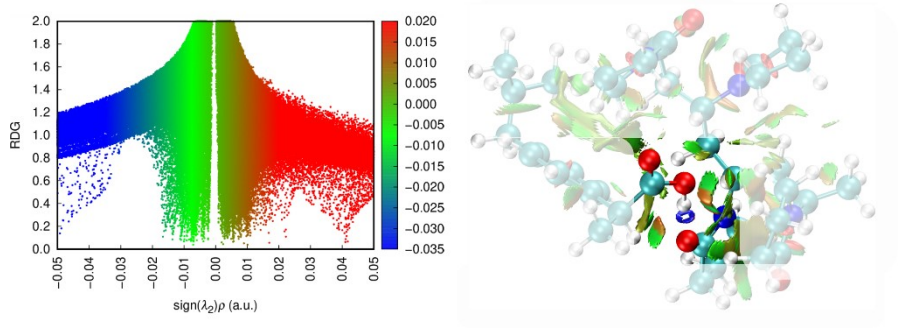

Figure S23. Analysis of non-covalent interactions of a PVP oligomer surrounding the carboxyl moiety of IBU in terms of critical points of the reduced density gradient plot and the signed electron density. Conformation with a strong $H_O^{IBU}…O_C^{PVP}$ hydrogen bond (dark blue RDG isosurface). Attractive dispersion interactions depicted with green isosurfaces, repulsive interactions depicted with yellow to red shades.

S4. Inner dynamics

This section contains additional simulation results on inner dynamics of bulk mixtures of target API and polymers. Plots of molecular mean-square displacements a functions of simulation time are given below.

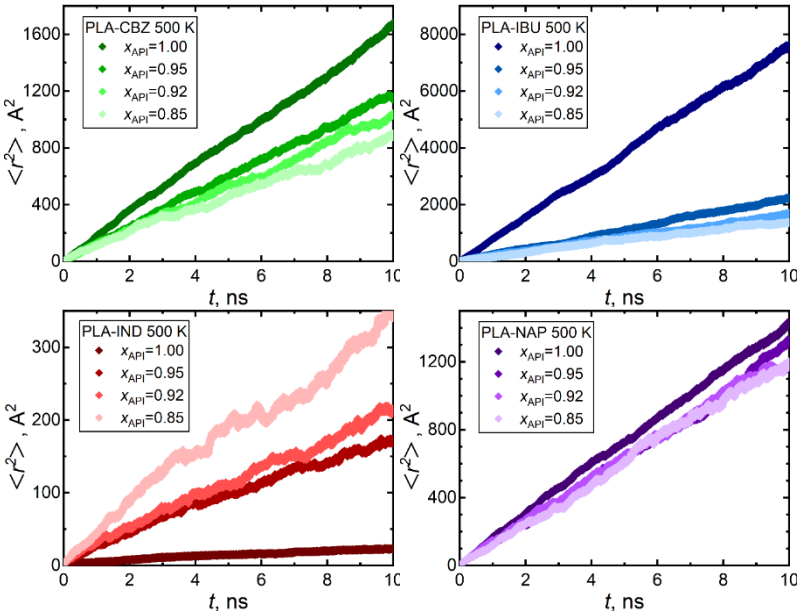

Figure S24. Mean-square displacements of API molecules as functions of time in various bulk systems simulated at 500 K.

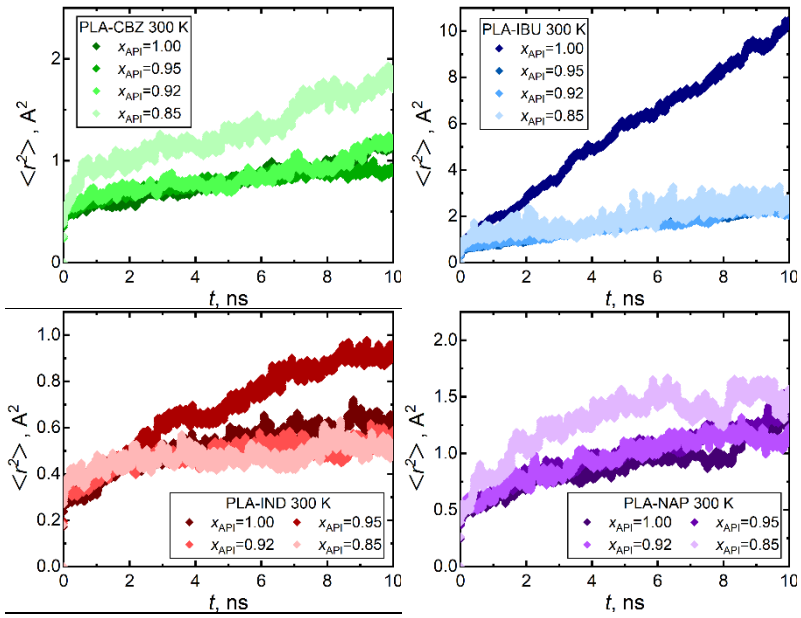

Figure S25. Mean-square displacements of API molecules as functions of time in various bulk systems simulated at 300 K.

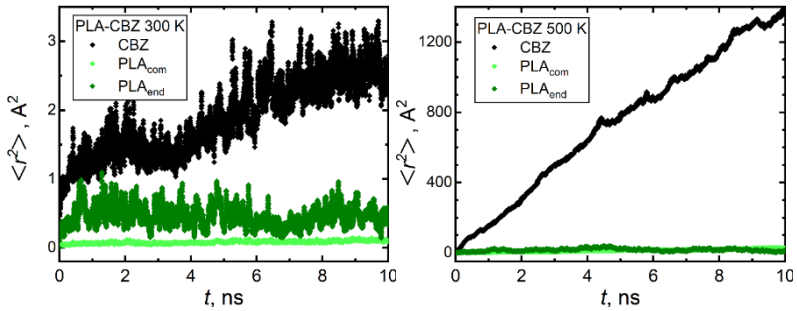

Figure S26. Mean-square displacements of CBZ molecules, centers of mass (com) and end groups of PLA chains as functions of time in bulk mixtures with x_{API}=0.85 simulated at 300 K and at 500 K. Data smoothed using a 10 ps running average window.

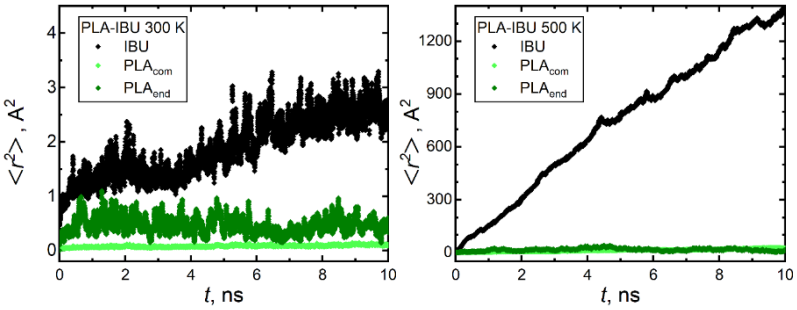

Figure S27. Mean-square displacements of IBU molecules, centers of mass (com) and end groups of PLA chains as functions of time in bulk mixtures with x_{API}=0.85 simulated at 300 K and at 500 K. Data smoothed using a 10 ps running average window.

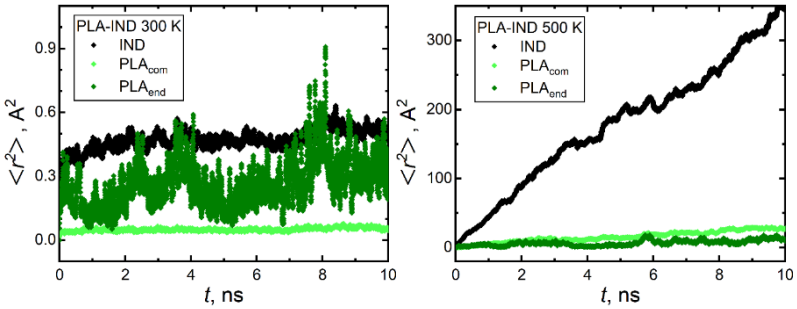

Figure S28. Mean-square displacements of IND molecules, centers of mass (com) and end groups of PLA chains as functions of time in bulk mixtures with x_{API}=0.85 simulated at 300 K and at 500 K. Data smoothed using a 10 ps running average window.

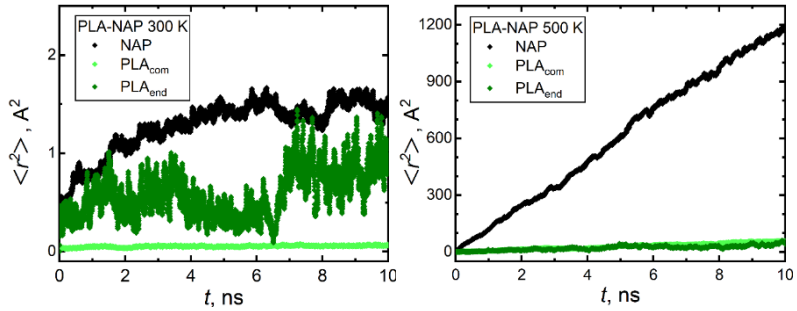

Figure S29. Mean-square displacements of NAP molecules, centers of mass (com) and end groups of PLA chains as functions of time in bulk mixtures with x_{API}=0.85 simulated at 300 K and at 500 K. Data smoothed using a 10 ps running average window.

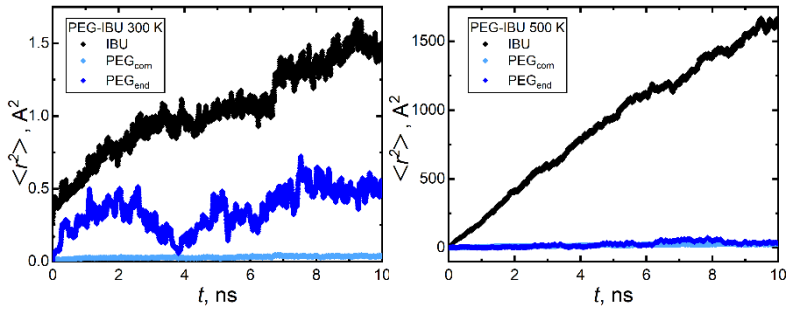

Figure S30. Mean-square displacements of IBU molecules, centers of mass (com) and end groups of PEG chains as functions of time in bulk mixtures with x_{API}=0.85 simulated at 300 K and at 500 K. Data smoothed using a 20 ps running average window.

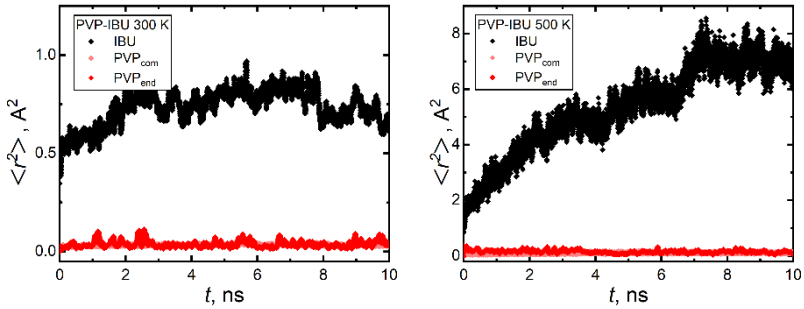

Figure S31. Mean-square displacements of IBU molecules, centers of mass (com) and end groups of PVP chains as functions of time in bulk mixtures with x_{API}=0.85 simulated at 300 K and at 500 K. Data smoothed using a 20 ps running average window.

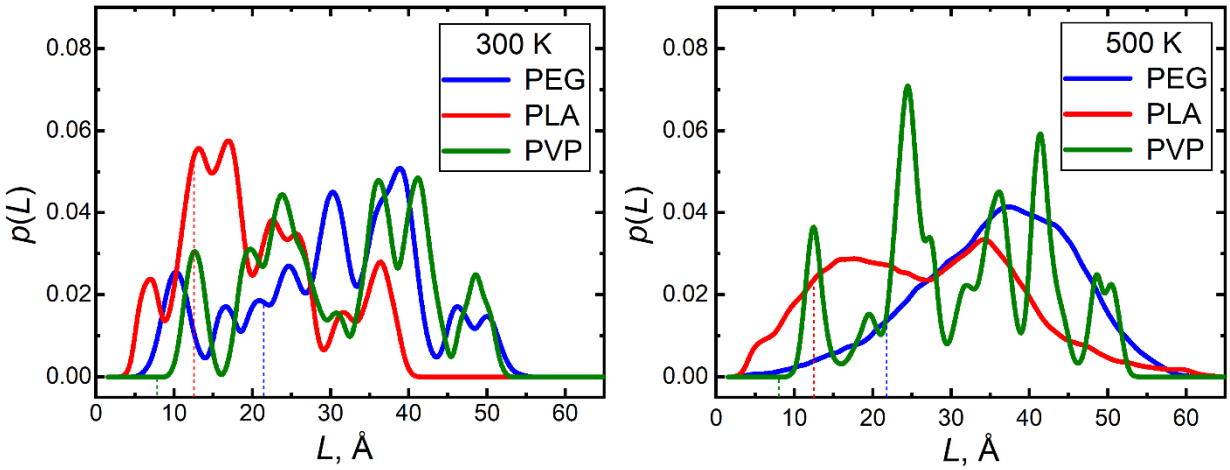

Figure S32. Histograms of the occurrence $p(L)$ of instantaneous end-to-end distances L of individual polymer chains derived from the MD simulation of bulk mixtures with the ibuprofen content x_{API}=0.85. Vertical dashed lines denote the end-to-end distance in the original globular conformation that was packed upon building of the simulation box.

S5. Glass-transition temperatures

This section contains additional simulation results on the glass-transition temperatures of bulk one-mixtures of target API and polymers. Numerical lists of the calculated results are given below.

Table S2
Results on T_g (in K) determined from individual simulated cooling runs for the considered mixtures the composition of which always corresponds to x_{API}=0.85.

System	Run 1	Run 2	Run 3	Run 4	Run 5	Average
PLA-CBZ	362.0 ± 1.9	373.2 ± 1.2	380.3 ± 1.9	363.9 ± 1.5	373.0 ± 0.4	371 ± 8
PLA-IBU	364.0 ± 0.3	362.2 ± 0.4	362.2 ± 1.7	364.8 ± 0.3	360.2 ± 2.4	363 ± 3
PLA-IND	378.6 ± 5.4	369.0 ± 7.1	375.1 ± 2.4	390 ± 6.0	385.6 ± 3.4	380 ± 14
PLA-NAP	374.4 ± 0.4	364.4 ± 0.4	381.0 ± 0.6	366.5 ± 0.4	364.6 ± 0.3	370 ± 8

Table S3
Comparison of simulated T_g (in K) values obtained in this work for pure compounds with previously determined experimental data.

System	Simulation	Experiment	Source
PLA	369 ± 3	333	ref. [1] and refs. therein
CBZ	384 ± 13	315	ref. [2]
IBU	295 ± 13	228	ref. [2]
IND	388 ± 21	313	ref. [2]
NAP	343 ± 13	278	ref. [2]

1. Klajmon, M.; Aulich, V.; Ludík, J.; Červinka, C., Glass Transition and Structure of Organic Polymers from All-Atom Molecular Simulations. *Industrial & Engineering Chemistry Research* **2023,** *62* (49), 21437-21448.
2. Štejfa, V.; Pokorný, V.; Mathers, A.; Růžička, K.; Fulem, M., Heat capacities of selected active pharmaceutical ingredients. *The Journal of Chemical Thermodynamics* **2021,** *163*, 106585.